

Double-layer microwave absorber based on nanocrystalline CoFe_2O_4 and $\text{CoFe}_2\text{O}_4/\text{PANI}$ multi-core/shell composites

YEWEN XU¹, GUOZHU SHEN^{2,*}, HONGYAN WU², BIN LIU², XUMIN FANG¹,
DING ZHANG¹, JUN ZHU¹

¹Science and Technology on Near-Surface Detection Laboratory, Wuxi 214035, China

²School of Physics and Optoelectronic Engineering, Nanjing University of Information Science & Technology, Nanjing 210044, China

Organic-inorganic nano- $\text{CoFe}_2\text{O}_4/\text{PANI}$ (polyaniline) multi-core/shell composites have been successfully synthesized by chemical oxidative polymerization of aniline. The characterization results showed that the ferrite nanocrystals were efficiently embedded in PANI. The electromagnetic parameters of the composites were measured by a vector network analyser in the frequency range of 2 GHz to 18 GHz. Double-layer absorbers based on the $\text{CoFe}_2\text{O}_4/\text{PANI}$ composite (matching layer) and calcined CoFe_2O_4 ferrite (absorbing layer) have been designed. The reflection loss of the microwave absorbers of both single layer and double-layer with a total thickness of 2.0 mm and 2.5 mm was calculated according to transmission-line theory. The results indicated that the minimum reflection loss of the $\text{CoFe}_2\text{O}_4/\text{PANI}$ composite was -19.0 dB at 16.2 GHz at the thickness of 2.0 mm and -23.6 dB at 13.1 GHz at the thickness of 2.5 mm, respectively. The minimum reflection loss for double-layer absorbers reached -28.8 dB at 16.2 GHz at the total thickness of 2.0 mm, and -31.1 dB at 12.8 GHz at the total thickness of 2.5 mm. The absorption bandwidth under -10 dB was 4.2 GHz (13.8 GHz to 18.0 GHz) and 5.5 GHz (10.3 GHz to 15.8 GHz), respectively. The results show that the reflection loss and absorption bandwidth of the double-layer absorbers are obviously enhanced compared to corresponding single layer absorbers.

Keywords: *cobalt ferrite; polyaniline; double-layer absorber; reflection loss*

© Wrocław University of Science and Technology.

1. Introduction

In recent years, electromagnetic (EM) pollution with the fast development of detection, information and communication technology in industrial, commercial and military applications, is becoming more and more serious. EM radiation can not only severely interrupt electronic controlling systems but also do harm to the health of human beings. To solve this problem, much attention has been paid to find EM wave absorbers. Absorption properties of absorbers mainly depend upon the relative complex permittivity and permeability of materials. Nowadays, various kinds of materials, such as dielectric, magnetic and conducting materials, have been studied, developed and applied in this field. The dielectric materials as EM

wave absorbers mainly include some nonmagnetic metal oxides and inorganic salts such as ZnO [1, 2], MnO_2 [3], BaTiO_3 [4, 5]. Magnetic absorbers belong to the class of magnetic loss materials including ferrites, metals Fe, Co, Ni and carbonyl iron [6–9]. Ferrites, including soft magnetic and hard magnetic ferrites are better candidates for absorbing materials because of the high magnetic loss, though their dielectric loss has never been neglected, and have been intensively investigated [10–12]. Currently, the research interest in ferrite materials is to enhance the absorption intensity and broaden absorption bandwidth under -10 dB in the microwave band by doping [13–15] and controlling particle morphology and size [16–19]. Complex permeability of magnetic metal materials may decrease due to eddy current phenomena induced by electromagnetic waves, therefore, they usually form composites with other dielectric and magnetic

*E-mail: shengz@nuist.edu.cn

loss materials [20–22]. Similarly, the conducting materials acting as EM wave absorbers usually combine with some magnetic loss materials. They mainly include some conductive polymers such as polyaniline and polypyrrole [23–25] and carbonaceous materials, such as carbon nanotubes [26, 27], graphene [28, 29], carbon fibers [30, 31], mesoporous carbon [32, 33], and so on. Furthermore, multilayer structure absorbers are attracting great attention due to their more adjustable variable parameters than those of single layer absorbers [34–36]. Ni et al. [37] reported that double-layer composites consisting of barium titanate/carbon nanotubes 30 wt.% (absorbing layer) with a thickness of 1.0 mm and barium titanate 30 wt.% (matching layer) with a thickness of 0.3 mm showed a minimum reflection loss of -63.7 dB, and the double-layer absorber had a much better absorption characteristics than the corresponding single layer absorber. Another double-layer absorber using ferrite as a matching layer and carbonyl iron as absorbing layer was studied by Liu et al. [38]. The results showed that the absorber not only greatly expanded the absorption bandwidth but also decreased the reflectance peak. Therefore, better absorption properties and wider absorption bandwidth can be expected by appropriate designing layer material, thickness, order, and so on. PANI materials are better candidates for multilayer absorbers [39], because their dielectric constant can be easily adjusted by doping, and the morphology and size of the polymer particles can be easily controlled by changing reaction conditions. In addition, the magnetic properties can be tailored by appropriate preparing ferrite/PANI composite. To the best of our knowledge, reports on double-layer microwave absorbing materials based on the PANI and spinel ferrite materials are still very limited.

In this work, spinel cobalt ferrite CoFe_2O_4 nanocrystals were synthesized by co-precipitation method, and the $\text{CoFe}_2\text{O}_4/\text{PANI}$ multi-core/shell composites were prepared by chemical oxidative polymerization of aniline. Double-layer microwave absorbers based on the calcined CoFe_2O_4 and $\text{CoFe}_2\text{O}_4/\text{PANI}$ multi-core/shell composites were designed to achieve higher microwave absorption.

2. Experimental

2.1. Materials

Ferric nitrate nonahydrate ($\text{Fe}(\text{NO}_3)_3 \cdot 9\text{H}_2\text{O}$ Shantou Xilong Chemical Co., Ltd.), cobalt chloride ($\text{CoCl}_2 \cdot 9\text{H}_2\text{O}$, Shanghai Zhenxin Reagent Factory), ammonia (Yangzhou Hubao Chemical Reagents Co., Ltd.), aniline (Chengdu Kelong Chemical Co., Ltd.), p-toluene sulfonic acid (PTSA, $\text{C}_7\text{H}_8\text{O}_3\text{S} \cdot \text{H}_2\text{O}$) and ammonium persulfate (APS, $(\text{NH}_4)_2\text{S}_2\text{O}_8$) were purchased from Shanghai Lingfeng Chemical Reagent Co., Ltd. All chemicals were of analytical grade and used without further purification, and all solutions were prepared with deionized water.

2.2. Synthesis of spinel cobalt ferrite nanoparticles

Cobalt ferrite nanopowder was synthesized via co-precipitation method. In a typical synthesis, 5 mmol $\text{Fe}(\text{NO}_3)_3 \cdot 9\text{H}_2\text{O}$ and 2.5 mmol $\text{CoCl}_2 \cdot 2\text{H}_2\text{O}$ were dissolved in 200 mL deionized water with magnetic stirring at room temperature. When the solution was heated to 60°C , 5 mL ammonia solution was added to the salt solution. Then, the mixture was sealed and heated at 80°C for 2 h under vigorous stirring. The obtained precipitate (denoted as S1) was centrifuged and thoroughly washed three times with deionized water, and then washed with ethanol. Finally, the precipitate was dried at 80°C overnight. A part of sample S1 was calcined at 500°C for 5 h in air atmosphere. The prepared sample was denoted as S2.

2.3. Preparation of $\text{CoFe}_2\text{O}_4/\text{PANI}$ multi-core/shell composites

The $\text{CoFe}_2\text{O}_4/\text{PANI}$ multi-core/shell composite was prepared by chemical oxidative polymerization of aniline in the presence of PTSA using APS. The synthesis process was as follows: 15 mmol PTSA, 9 mmol APS and 100 mg S1 powder were added into 200 mL deionized water in an ice-water bath with mechanical stirring for 1 h. Then the aniline solution (9 mmol aniline was dissolved in 50 mL deionized water) was added into the mixture in an ice-water bath under continuous

stirring for additional 8 h. The final product was centrifuged and washed three times with deionized water, then dried at 80 °C for 24 h. The prepared sample was denoted as S3. The sample S4 was prepared by changing CoFe_2O_4 doses (386 mg), while the preparative procedure was the same as that of the sample S3.

2.4. Characterization and measurement

The X-ray diffraction (XRD) patterns were collected on a Thermo Scientific ARL X'TRA Powder Diffractometer (CuK α radiation, 40 kV, 40 mA, $\lambda = 1.5406 \text{ \AA}$). Transmission electron microscope (TEM) images were taken on Hitachi H-800 and JEM-2100F. Scanning electron microscope (SEM) images were obtained on a Hitachi SU3500 with accelerating voltages of 30.0 kV and a thin layer of gold film was sprayed on the samples before the characterization. The magnetic hysteresis loops were measured with a vibrating sample magnetometer (VSM) (Lakeshore 7300) operating at room temperature. The electromagnetic parameters (relative complex permittivity and permeability) of the samples were determined by a vector network analyzer (Agilent Technologies E5071C) in the frequency range of 2 GHz to 18 GHz. In order to measure the electromagnetic parameters, the samples composed of powder-paraffin wax composites with the weight ratio of powder sample to paraffin wax of 10:9 for CoFe_2O_4 /PANI and 7:3 for calcined CoFe_2O_4 were prepared by homogeneous mixing, and then pressed into toroidal-shaped samples with the outer and inner diameters of 7.0 mm and 3.0 mm, respectively.

3. Results and discussion

3.1. Characterization of samples

XRD patterns of the prepared samples are illustrated in Fig. 1. The samples S1 and S2 show that all the diffraction peaks can be well indexed to face-centered cubic cobalt ferrite (CoFe_2O_4) phase (JCPDS Card No. 22-1086) with a space group of Fd3m. Full width at half-maximum of the calcined sample S2 is smaller compared to that of S1. The average crystallite size of cobalt ferrite is 7.2

and 11.5 nm for samples S1 and S2, respectively. According to Scherrer's formula $D = k\lambda/\beta\cos\theta$, where λ is the X-ray wavelength of CuK α radiation (1.54 Å), k is the shape factor, to which a value of 0.89 can be assigned if the shape is unknown, θ is the Bragg angle and β is the full-width at half-maximum intensity of the peak. The sample S3 has two broad peaks with 2θ centered at 20.3° and 25.3°, which are usually ascribed to the periodicity parallel and perpendicular to the PANI chains, respectively [39, 40]. It is also found that the peaks get weaker with increasing ferrite ratio in the composites, as shown in sample S4, and no peaks of any other crystal phases can be observed besides the CoFe_2O_4 in the sample S3 and S4, confirming only CoFe_2O_4 crystal dispersed in the PANI matrix.

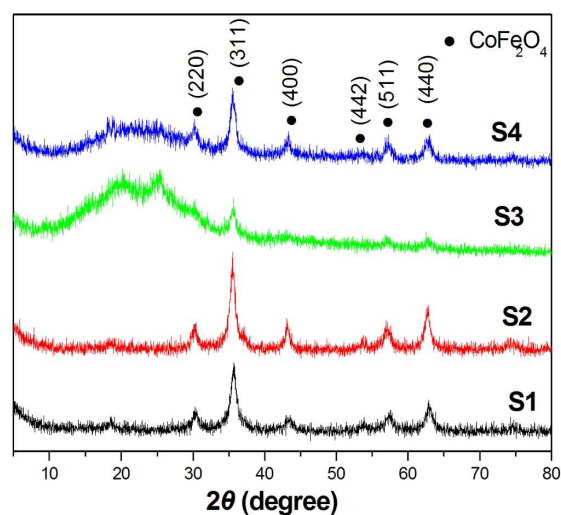


Fig. 1. XRD patterns of samples S1, S2, S3 and S4.

The morphologies of the cobalt ferrite CoFe_2O_4 and CoFe_2O_4 /PANI composite particles were examined by TEM and SEM. It can be observed from Fig. 2a that the size of ferrite CoFe_2O_4 S1 particles synthesized at 80 °C is 8 nm to 10 nm, which is similar to the result obtained by El-Okri *et al.* [41]. Fig. 2b shows the TEM image of CoFe_2O_4 S2 calcined at 500 °C. The size of the particles is about 15 nm. It can be seen that the morphology of CoFe_2O_4 /PANI composite particles is nearly spherical, and the size of the spheres ranges between 40 nm and 100 nm (Fig. 2c and Fig. 2d). It is

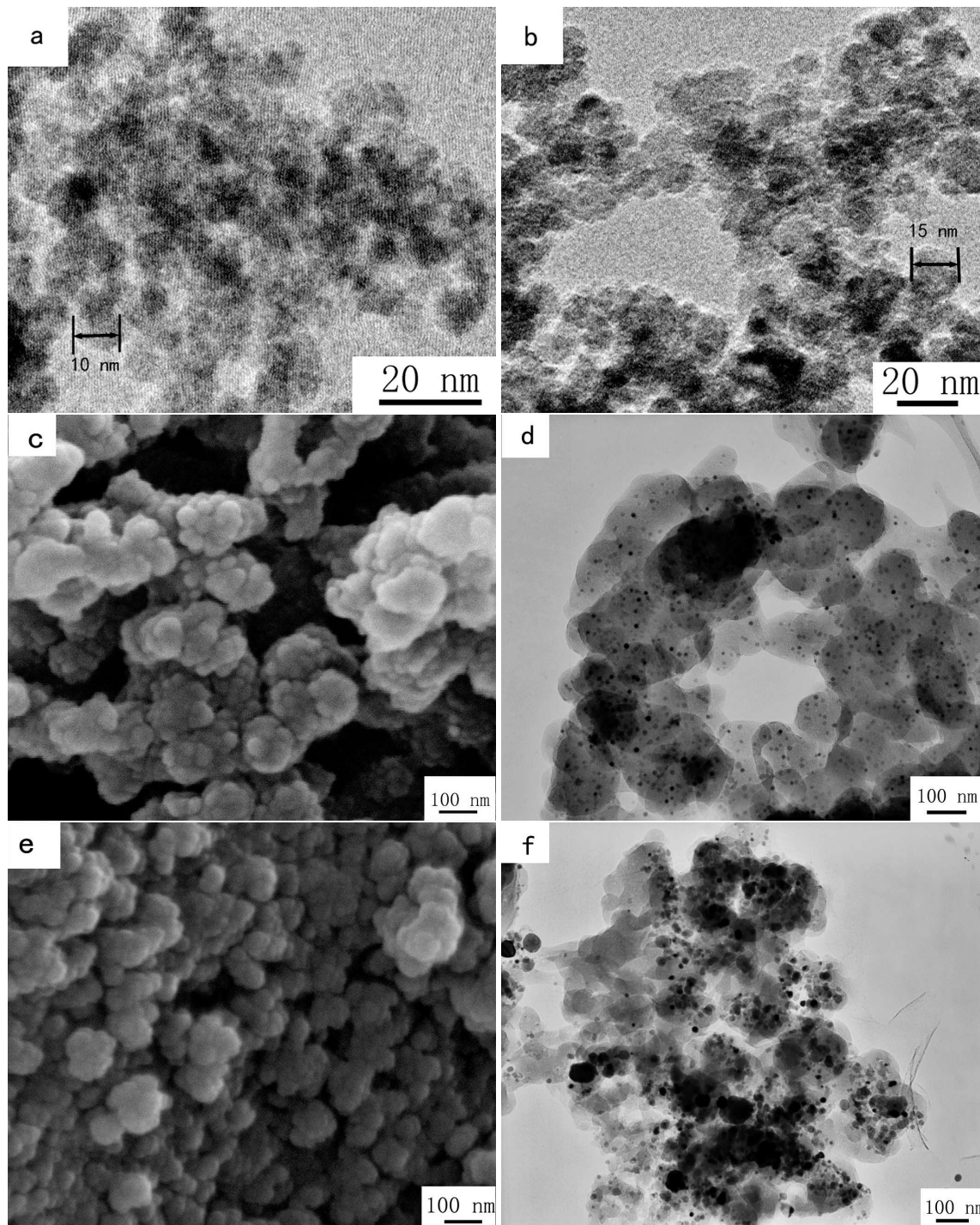


Fig. 2. TEM (a, b, d, f) and SEM (c, e) images of the sample S1 (a), S2 (b), S3 (c, d) and S4 (e, f).

seldom found that the surfaces of spherical particles are coated by any smaller particles, therefore the inorganic ferrite nanoparticles should embed into the PANI polymeric matrix. Similar result can

also be found from the TEM image in Fig. 2d. The image clearly indicates that the CoFe_2O_4 nanoparticles are uniformly dispersed in the PANI particles, and no aggregation of the nanoparticles

can be found. Fig. 2e and Fig. 2f show that the grain morphologies of sample S4 are similar to that of sample S3. However, from Fig. 2f, it can be found that some ferrite nanoparticles in PANI matrix have aggregated together. That is to say, uniform dispersion of ferrite nanoparticles is difficult to achieve with the increase of CoFe_2O_4 dosage in the PANI (from 100 mg to 386 mg).

On the basis of the above characterization and analyses, the synthesis procedure for the nano- CoFe_2O_4 /PANI multi-core/shell composites can be schematically illustrated in Fig. 3.

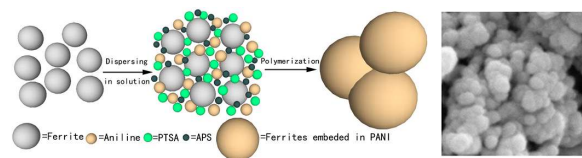


Fig. 3. Schematic illustration of the synthesis process of CoFe_2O_4 /PANI multi-core/shell composites.

Magnetic measurements of samples S2, S3 and S4 were performed using VSM technique. The magnetic hysteresis loops at room temperature versus applied magnetic field up to 9 kG are shown in Fig. 4a. Obviously, all the samples show soft magnetic performance. The saturation magnetization (M_s) is about 30.5 emu/g, 2.0 emu/g and 7.9 emu/g for the sample S2, S3 and S4, respectively. The higher M_s value of S4 than that of S3 is due to increased CoFe_2O_4 content in the CoFe_2O_4 /PANI composite. The highest M_s value for the sample S2 is attributed to the absence of PANI in sample S2 and high degree of crystallization of ferrite derived from the high calcination temperature. The coercivity (H_c) value for the sample S2, S3 and S4 is 201 G, 236 G and 147 G, respectively. To clearly compare the H_c values, the zoomed middle part of the hysteresis loops is shown in Fig. 4b. The highest H_c value of S3 resulted from small size effect or the nanoregime (the ferrite nanoparticles of sample S3 dispersed uniformly in the PANI matrix, which is different from that of sample S4 where the aggregation of nanoparticles is serious as shown in TEM images). According to the nanoregime, magnetic nanomaterials reveal a changeover from multi-domain nature to single

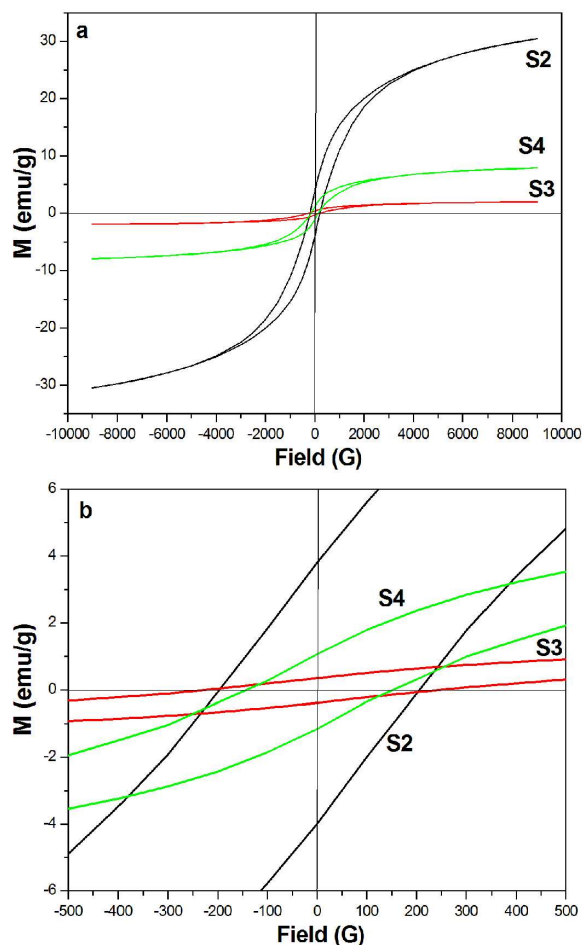


Fig. 4. Hysteresis loops at room temperature for sample S2, S3 and S4.

domain nature, and the coercivity of nanomaterial is mainly attributed to the demagnetization caused by single domain rotation. However, the H_c value of S2 is co-determined by the heat treatment temperature and particle size. The more details about magnetic properties of nanomaterials have been discussed by Pradeep *et al.* [42].

3.2. Microwave electromagnetic properties

The real parts (ϵ' and μ') of complex permittivity and permeability represent the storage of electric and magnetic energies, respectively, while the imaginary parts (ϵ'' and μ'') symbolize the loss and dissipation of both energies. The variation of relative complex permittivity and permeability

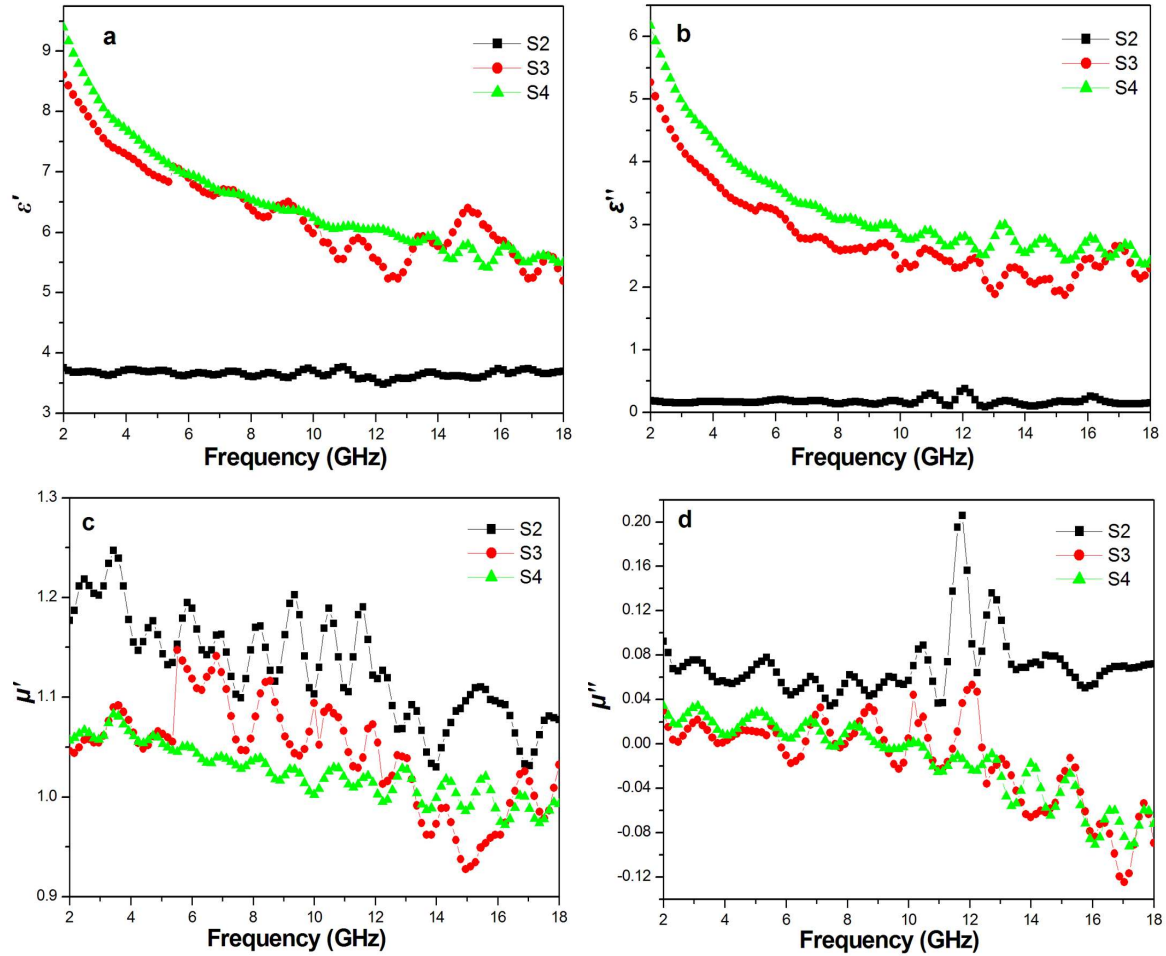


Fig. 5. Variation of complex permittivity and permeability of sample S2, S3 and S4 with frequency.

of the samples S2, S3 and S4 with frequency is shown in Fig. 5. It can be found that the values of ϵ' and ϵ'' of the sample S2 and S3 decrease with the increasing frequency, and fluctuate in the high frequency range as shown in Fig. 5a and 5b. Generally, the ϵ' and ϵ'' of sample S4 are higher than that of S3 almost in the whole frequency range. The dielectric properties of materials result mainly from the intrinsic electric dipole polarization and interfacial polarization. The more addition of ferrite nanoparticles can introduce more additional interfaces and more polarization charges. Therefore, the values of ϵ' and ϵ'' increase with increasing ferrite ratio. Meanwhile, for PANI composite, the contribution of electric conductance loss to ϵ'' cannot be neglected because of the electric conduction of PANI. The real part ϵ' of pure ferrite sample S2 is

the lowest and remains constant at approximately 3.65 in the whole frequency range, while three obvious peaks of ϵ'' for S2 can be observed at about 10.9, 12.0 and 16.1 GHz, respectively.

The dependence of μ' and μ'' on frequency is shown in Fig. 5c and Fig. 5d. Clearly, μ' and μ'' of the calcined ferrite sample S2 are higher than those of the other two samples. The high values of μ' and μ'' mainly derive from strong magnetic properties of S2. Additionally, two strong resonance peaks of μ'' can be observed at 11.7 GHz and 12.8 GHz. These resonance peaks may result from the exchange resonance of magnetic materials according to the Aharoni's theory which has been reported in a previous report [43]. Fig. 5c and Fig. 5d also show that the μ' and μ'' values of S3 are

comparable with those of S4 in the whole frequency range. Furthermore, negative μ'' can be observed for S3 and S4 samples. The negative μ'' values can be considered as induced magnetic energy coming out of the absorbers. For conductive PANI composite, eddy current induced by electromagnetic waves can easily form, and then conversely induce new magnetic energy radiated out the absorber.

To further investigate the dielectric and magnetic loss properties, the reflection loss (R) of these composites was calculated according to transmission-line theory.

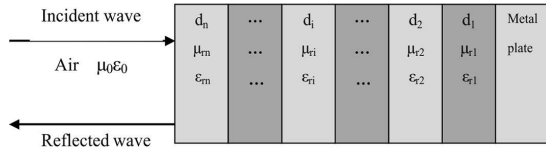


Fig. 6. Sketch map of incidence of electromagnetic wave in multi-layer absorber.

The geometry of a multi-layer microwave absorber is shown in Fig. 6. An electromagnetic wave with unit amplitude propagating along the positive z -direction is incident normally to the absorber and gives rise to a series of waves traveling in the positive and reflected wave traveling in the negative z -direction within the layers.

Let d_i , η_i and γ_i denote the thickness, complex intrinsic impedance and propagation constants of the i th layer, respectively ($i = 1, 2, 3, \dots, n$). ϵ_0 , μ_0 are the permittivity and permeability of free space. According to transmission-line theory [44, 45], the wave impedance Z_i for the i -th layer is given by:

$$Z_i = \eta_i \frac{Z_{i-1} + \eta_i \tanh(\gamma_i d_i)}{\eta_i + Z_{i-1} \tanh(\gamma_i d_i)} \quad (1)$$

where η_i and γ_i are given as:

$$\eta_i = \eta_0 \sqrt{\frac{\mu_{ri}}{\epsilon_{ri}}} \quad (2)$$

$$\gamma_i = j \frac{2\pi f}{c} \sqrt{\mu_{ri} \epsilon_{ri}} \quad (3)$$

where η_0 is a characteristic impedance of the free space and ϵ_{ri} , μ_{ri} are the relative complex permittivity and permeability of the i^{th} layer, respectively.

f is the frequency and c is the velocity of light in free space.

Since the microwave absorber is deposited on a metal conductor, thus the impedance of the short circuited first layer is given by:

$$Z_1 = \eta_1 \tanh(\gamma_1 d_1) \quad (4)$$

where η_1 and γ_1 are intrinsic impedance and complex propagation constants of the first layer.

Using equation 1 to equation 4, the overall reflection coefficient for a multilayer absorber at an air-absorber interface is given as:

$$\Gamma = \left| \frac{Z_n - \eta_0}{Z_n + \eta_0} \right| \quad (5)$$

Thus, the reflection loss R of the electromagnetic wave incident normal to the planar multi-layer structure can be expressed as:

$$R = 20 \lg |\Gamma| \quad (6)$$

Using equation 2 to equation 6, the R for a single-layer coating is given as:

$$R = 20 \lg \left| \frac{\sqrt{\frac{\mu_r}{\epsilon_r}} \tanh(j \frac{2\pi f d}{c} \sqrt{\mu_r \epsilon_r}) - 1}{\sqrt{\frac{\mu_r}{\epsilon_r}} \tanh(j \frac{2\pi f d}{c} \sqrt{\mu_r \epsilon_r}) + 1} \right| \quad (7)$$

Fig. 7 shows the calculated microwave reflection loss R of a single-layer coating with the thickness of 2.0 mm and 2.5 mm according to equation 7, respectively. The R of both S3 and S4 gradually decreases and achieves minimum value of -17.4 dB at 17.0 GHz and -19.0 dB at 16.2 GHz for the thickness $d = 2.0$ mm, and the effective absorption band width under -10 dB is 3.1 GHz (14.9 GHz to 18.0 GHz) and 3.9 GHz (14.1 GHz to 18.0 GHz), respectively, as shown in Fig. 7a. It is also found that the locations of the adsorption peaks of S3 and S4 samples correspond to that of the dielectric loss tangent ($\tan \delta_e$) peaks as shown in Fig. 7c. The results illustrate that the microwave absorption mainly results from the dielectric loss. Fig. 7b shows the minimum R value is -16.6 dB at 12.1 GHz and -23.6 dB at 13.1 GHz for both samples with the thickness

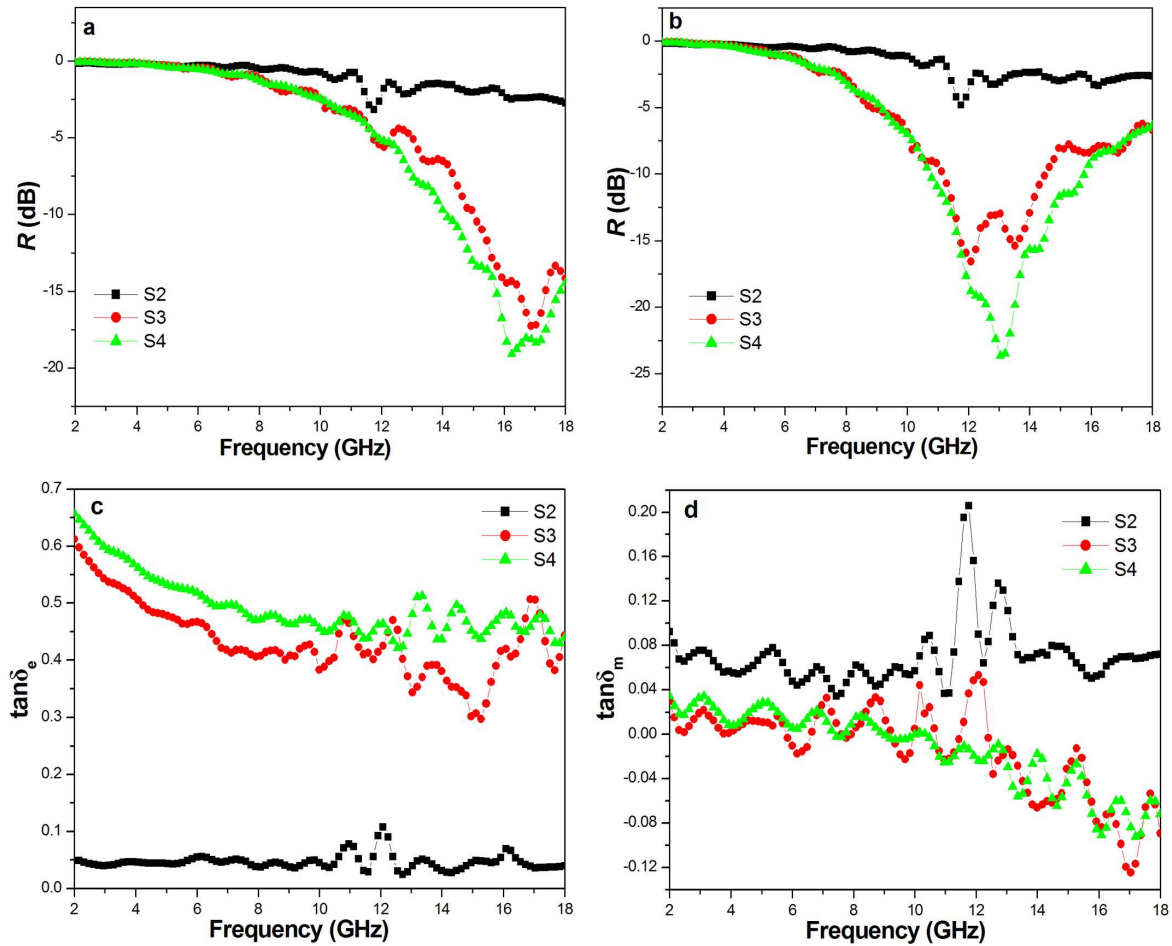


Fig. 7. Absorption curves of the layers with thickness $d = 2.0$ mm (a), 2.5 mm (b), and variation of dielectric loss tangent (c) and magnetic loss tangent (d) of sample S2, S3 and S4 with frequency.

$d = 2.5$ mm, and the effective absorption bandwidth is 3.4 GHz (11.1 GHz to 14.5 GHz) and 3.7 GHz (10.8 GHz to 14.5 GHz), respectively. Compared to the R curves in Fig. 7a, the location of the absorption peaks for the sample S3 and S4 shifts to lower frequency with the thickness increasing from 2.0 to 2.5 mm. For the calcined ferrite sample S2, the microwave adsorption is weak in the whole frequency range, and the absorption mainly comes from the magnetic loss as shown in Fig. 7a, Fig. 7b and Fig. 7d.

In order to improve the microwave absorption properties, the double-layer absorber, composed of the matching layer and absorbing layer, has been designed and R values were calculated according to

equation 1 to equation 6. Due to the excellent microwave absorption property of sample S4, it was selected to act as a matching layer. The Fig. 8a and Fig. 8b show the R of double-layer absorber whose absorbing layer (layer 1) is ferrite sample S2 and matching layer (layer 2) is $\text{CoFe}_2\text{O}_4/\text{PANI}$ composite sample S4 with the total thickness of 2.0 mm and 2.5 mm, respectively. The layer structure and reflection loss results are summarized in Table 1 (including single layer absorber S2-S4), where the double-layer absorber samples are denoted as S5-S11. For the double-layer absorber with a total thickness of 2.0 mm (S5-S7), it can be found that the minimum R value is -28.8 dB at 16.2 GHz, and the effective bandwidth under -10 dB is 4.2 GHz (13.8 GHz to 18.0 GHz) when

Table 1. Microwave absorption properties of single layer (S2-S4) and double-layer (S5-S11) absorbers with total thickness of 2.0 mm and 2.5 mm.

Sample	Material	Thickness [mm]	Total thickness [mm]	Min. R [dB]	R peak [GHz]	Bandwidth R < -10 dB [GHz]
S2	Calcined ferrite	2.0	2.0	-3.2	11.7	-
		2.5	2.5	-4.8	11.8	-
S3	Ferrite/PANI composite	2.0	2.0	-17.4	17.0	14.9 – 18.0 (3.1)
		2.5	2.5	-16.6	12.1	11.1 – 14.5 (3.4)
S4	Ferrite/PANI composite	2.0	2.0	-19.0	16.2	14.1 – 18.0 (3.9)
		2.5	2.5	-23.6	13.1	10.8 – 14.5 (3.7)
S5	Layer 1: S2	0.5	2.0	-28.8	16.2	13.8 – 18.0 (4.2)
	Layer 2: S4	1.5				
S6	Layer 1: S2	1.0	2.0	-22.3	16.2	14.2 – 18.0 (3.8)
	Layer 2: S4	1.0				
S7	Layer 1: S2	1.5	2.0	-11.6	17.3	15.9 – 18.0 (2.1)
	Layer 2: S4	0.5				
S8	Layer 1: S2	0.5	2.5	-28.8	12.8	10.3 – 15.8 (5.5)
	Layer 2: S4	2.0				
S9	Layer 1: S2	1.0	2.5	-31.1	12.8	10.3 – 15.8 (5.5)
	Layer 2: S4	1.5				
S10	Layer 1: S2	1.5	2.5	-22.4	13.2	11.1 – 15.8 (4.7)
	Layer 2: S4	1.0				
S11	Layer 1: S2	2.0	2.5	-11.2	11.7	11.5 – 12.0 (0.5)
	Layer 2: S4	0.5				

the thickness of layer 1 is 0.5 mm and the thickness of layer 2 is 1.5 mm (sample S5). It can be also observed that the microwave absorption properties are gradually weakened with the thickness of layer 2 decreasing from 1.5 mm to 0.5 mm. The similar variation tendency can be observed for the double-layer absorber (S8-S11) with a total thickness of 2.5 mm. When the thickness of layer 1 and 2 is 1.0 mm and 1.5 mm (sample S9), respectively, the minimum R value and effective bandwidth is -31.1 dB at 12.8 GHz and 5.5 GHz (10.3 GHz to 15.8 GHz), respectively. From Fig. 8, it is also found that the absorption peaks shift to lower frequency as the total thickness increases from 2.0 mm to 2.5 mm, which is similar to that of the single layer absorbers. It can be found from the reflection loss results as shown in Table 1, that the reflection loss of a double-layer absorber is determined not only by the layer material but also the thickness of each layer. It is obvious that a great

improvement of microwave absorption properties compared with the single layer absorber has been obtained by designing the double-layer structure absorber with the matching layer $\text{CoFe}_2\text{O}_4/\text{PANI}$ and absorbing layer CoFe_2O_4 composites. It is worth noting that the increase of matching layer thickness is more beneficial to microwave absorption for a certain thickness of absorber when the matching layer is a high dielectric loss material and absorbing layer is a high magnetic loss material.

4. Conclusions

In summary, $\text{CoFe}_2\text{O}_4/\text{PANI}$ multi-core/shell composites as microwave absorbers have been successfully fabricated by chemical oxidative polymerization of aniline. The double-layer absorbers with a total thickness of 2.0 mm and 2.5 mm based on the materials were designed. The microwave absorption properties of the single- and

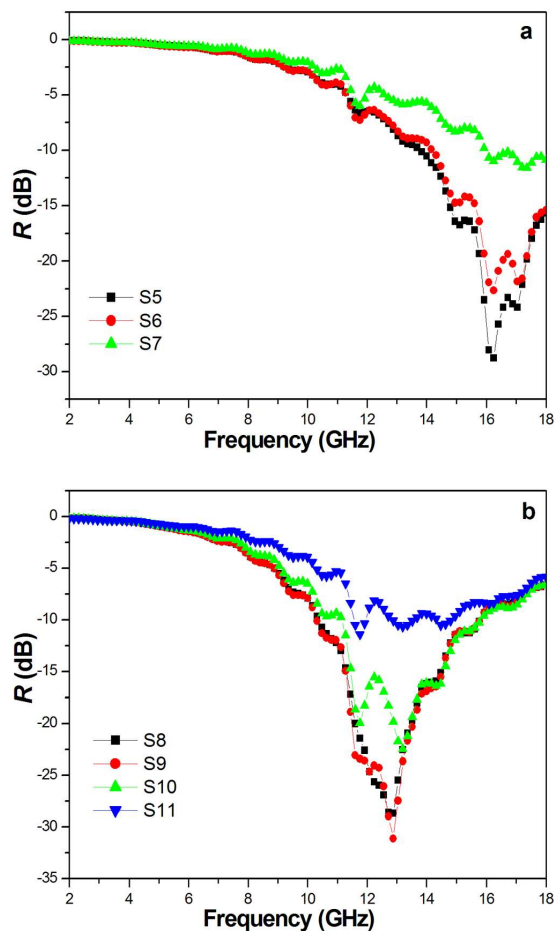


Fig. 8. Absorption curves of the double-layer absorbers with a total layer thickness $d = 2.0$ mm (a), 2.5 mm (b).

double-layer absorbers were investigated in the frequency range of 2 GHz to 18 GHz. The absorption properties and absorption bandwidth for the double-layer absorbers, where the absorbing layer is the calcined CoFe_2O_4 ferrite and matching layer is the $\text{CoFe}_2\text{O}_4/\text{PANI}$ composite are obviously improved compared to corresponding single layer absorbers. The minimum reflection loss for the double-layer absorber with a total thickness of 2.0 mm reaches -28.8 dB at 16.2 GHz and -31.1 dB at 12.8 GHz for the absorber with a total thickness of 2.5 mm. The absorption bandwidth under -10 dB is 4.2 GHz (13.8 GHz to 18.0 GHz) and 5.5 GHz (10.3 GHz to 15.8 GHz), respectively. In virtue of the facile and scalable synthesis, low-cost, and excellent microwave absorption performance,

the $\text{CoFe}_2\text{O}_4/\text{PANI}$ multi-core/shell composites are expected to have a great potential in microwave absorption applications.

Acknowledgements

This work has been supported by the Science and Technology on the Near-Surface Detection Laboratory, the Natural Science Foundation-Outstanding Youth Foundation of Jiangsu Province of China (BK20160091) and the Funds of National Natural Science Foundation of China (51405242).

References

- [1] HU Q., TONG G.X., WU W.H., LIU F.T., QIAN H.S., HONG D.Y., *CrystEngComm*, 15 (2013), 1314.
- [2] REN Y.Y., YANG L., WANG L.D., XU T.T., WU G.L., WU H.J., *Powder Technol.*, 281 (2015), 20.
- [3] WANG G.S., HE S., LUO X., WEN B., LU M.M., GUO L., CAO M.S., *RSC Adv.*, 3 (2013), 18009.
- [4] ABBAS S.M., CHANDRA M., VERMA A., CHATTERJEE R., GOEL T.C., *Compos. Part A-Appl. S.*, 37 (2006), 2148.
- [5] CHOI S.H., OH J.H., KO T., *J. Magn. Magn. Mater.*, 272 – 276 (2004), 2233.
- [6] WANG G.Q., WANG L.F., GAN Y.L., LU W., *Appl. Surf. Sci.*, 273 (2013), 744.
- [7] WANG A.M., WANG W., LONG C., LI W., GUAN J.G., GU H.S., XU G.X., *J. Mater. Chem. C*, 2 (2014), 3769.
- [8] LIU T., PANG Y., ZHU M., KOBAYASHI S., *Nanoscale*, 6 (2014), 2447.
- [9] WEN S.L., ZHAO X.C., LIU Y., CHENG J.W., LI H., *RSC Adv.*, 4 (2014), 40456.
- [10] ZHU W.M., WANG L., ZHAO R., REN J.W., LU G.Z., WANG Y.Q., *Nanoscale*, 3 (2011), 2862.
- [11] LIU J.L., ZHANG J., ZHANG P., WANG S.Y., LU C.Y., LI Y.Q., ZHANG M., *Mater. Lett.*, 158 (2015), 53.
- [12] GU X., ZHU W.M., JIA C.J., ZHAO R., SCHMIDT W., WANG Y.Q., *Chem. Commun.*, 47 (2011), 5337.
- [13] SILVA J.E.M., NASAR R.S., NASAR M.C., FIRME C.L., ARAUJO J.H., *J. Magn. Magn. Mater.*, 394 (2015), 274.
- [14] MOSLEH Z., KAMELI P., POORBAFERANI A., RANJBAR M., SALAMATI H., *J. Magn. Magn. Mater.*, 397 (2016), 101.
- [15] MENG P.Y., XIONG K., JU K., LI S.N., XU G.L., *J. Magn. Magn. Mater.*, 385 (2015), 407.
- [16] CHEN W., WU W.W., LIU S.Q., XU J.W., LIU D.S., WU X.H., ZHOU Y., WU J., *Mat. Sci. Semicon. Proc.*, 39 (2015), 544.
- [17] HUANG X.G., ZHANG J., LAI M., SANG T.Y., *J. Alloy. Compd.*, 627 (2015), 367.
- [18] REDDY M. P., MOHAMED A.M.A., *Micropor. Mesopor. Mat.*, 215 (2015), 37.
- [19] CAI X.D., WANG J.J., LIANG G.H., GUO J.S., HOU Y.S., GAO H.T., YU L., *J. Alloy. Compd.*, 636 (2015), 348.

- [20] SHEN X.Q., SONG F.Z., YANG X.C., WANG Z., JING M.X., WANG Y.D., *J. Alloy. Compd.*, 621 (2015), 146.
- [21] LI N., HU C.W., CAO M.H., *Phys. Chem. Chem. Phys.*, 15 (2013), 7685.
- [22] WANG H.Y., ZHU D.M., ZHOU W.C., LUO F., *J. Magn. Magn. Mater.*, 393 (2015), 445.
- [23] SHEN J.H., CHEN K.Y., LI L.C., WANG W.X., JIN Y., *J. Alloy. Compd.*, 615 (2014), 488.
- [24] LUO J.H., GAO D.D., *J. Magn. Magn. Mater.*, 368 (2014), 82.
- [25] LIU P.B., HUANG Y., *RSC Adv.*, 3 (2013), 19033.
- [26] LU M.M., CAO W.Q., SHI H.L., FANG X.Y., YANG J., HOU Z.L., JIN H.B., WANG W.Z., YUAN J., CAO M.S., *J. Mater. Chem. A*, 2 (2014), 10540.
- [27] LIU G., WANG L.Y., CHEN G.M., HUA S.C., GE C.Q., ZHANG H., WU R.B., *J. Alloy. Compd.*, 514 (2012), 183.
- [28] ZONG M., HUANG Y., ZHAO Y., SUN X., QU C.H., LUO D.D., ZHENG J.B., *RSC Adv.*, 3 (2013), 23638.
- [29] ZHU Z.T., SUN X., XUE H.R., GUO H., FAN X.L., PAN X.C., HE J.P., *J. Mater. Chem. C*, 2 (2014), 6582.
- [30] SHAH A., WANG Y.H., HUANG H., ZHANG L., WANG D.X., ZHOU L., DUAN Y.P., DONG X.L., ZHANG Z.D., *Compos. Struct.*, 131 (2015), 1132.
- [31] LI G., XIE T.S., YANG S.L., JIN J.H., JIANG J.M., *J. Phys. Chem. C*, 116 (2012), 9196.
- [32] ZHOU H., WANG J.C., ZHUANG J.D., LIU Q., *Nanoscale*, 5 (2013), 12502.
- [33] WU H.J., WANG L.D., GUO S.L., WANG Y.M., SHEN Z.Y., *Mater. Chem. Phys.*, 133 (2012), 965.
- [34] WEI C.Y., SHEN X.Q., SONG F.Z., ZHU Y.W., WANG Y.D., *Mater. Design*, 35 (2012), 363.
- [35] DAS S., NAYAK G.C., SAHU S.K., ROUSTRAY P.C., ROY A.K., BASKEY H., *J. Magn. Magn. Mater.*, 377 (2015), 111.
- [36] WANG T., QIAO L., HAN R., ZHANG Z.Q., *J. Magn. Magn. Mater.*, 324 (2012), 3209.
- [37] NI Q.Q., JET HONG MELVIN G., NATSUKI T., *Ceram. Int.*, 41 (2015), 9885.
- [38] LIU Y., LIU X.X., WANG X.J., *J. Alloy. Compd.*, 584 (2014), 249.
- [39] WANG H.J., LU Y., *Synthetic Met.*, 162 (2012), 1369.
- [40] GU H.B., WEI H.G., GUO J., HALDOLAARACHIGE N., YOUNG D.P., WEI S.Y., GUO Z.H., *Polymer*, 54 (2013), 5974.
- [41] EL-OKR M.M., SALEM M.A., SALIM M.S., EL-OKR R.M., ASHOUSH M., TALAAT H.M., *J. Magn. Magn. Mater.*, 323 (2011), 920.
- [42] PRADEEP A., PRIYADHARSINI P., CHANDRASEKARAN G., *J. Magn. Magn. Mater.*, 320 (2008), 2774.
- [43] AHARONI A., *J. Appl. Phys.*, 69 (1991), 7762.
- [44] SHEN G.Z., XU M., XU Z., *Mater. Chem. Phys.*, 105 (2007), 268.
- [45] MESHARAM M. R., AGRAWAL N.K., SINHA B., MISRA P.S., *J. Magn. Magn. Mater.*, 271 (2004), 207.

Received 2016-01-23
Accepted 2016-11-30